JEM Modeling and Measurement for Radar Target Identification

MARK R. BELL
Purdue University

ROBERT A. GRUBBS
Martin Marietta Corp.

The *jet engine modulation* (JEM) phenomenon, observed in radar returns from the rotating structure of jet engines, has been successfully exploited for aircraft target identification in a number of experimental radar systems. We develop a parametric model based on the periodic modulation of the scattered return, motivated by the potential reduction in time-on-target for reliable target identification provided by parametric models, as well as gaining insight into the JEM phenomenon. We then compare the model with JEM measurements made with an experimental radar system. Finally, we discuss the implications for JEM-based target identification systems.

I. INTRODUCTION

Jet engine modulation (JEM) of radar returns is a well-known phenomenon in the radar observation of jet aircraft [1, 2, 3, ch. 28]. The phenomenon occurs when a radar observes a jet airplane at an aspect angle that allows electromagnetic radiation to be backscattered from the moving parts of the compressor and blade assembly of the jet engine. The phenomenon has been observed at angles as great as 60° from a nose-on aspect between the radar and the observed aircraft [1]. Since the compressor and blade assembly are in (rotational) periodic motion with respect to the airframe of the observed aircraft, they impart a periodic modulation on the signal scattered from the engine structure in periodic motion. This periodic modulation has been known to have two significant consequences for the radar observation of incoming aircraft: the generation of "noise" that can sometimes impair the Doppler tracking of the observed target, and the generation of a radar signature that can be useful for target identification. Early studies focused on JEM-induced Doppler tracking noise, since the JEM-generated sidebands surrounding the Doppler frequency of the target airframe could confuse Doppler tracking algorithms attempting to track the target Doppler, or at least contribute to noisy estimates of the target Doppler [3, ch. 28]. This is not a significant problem in most modern radar tracking problems and is not considered further here.

We are concerned here with modeling the JEM phenomenon in order to better understand and exploit JEM target signatures. Investigations of the JEM or JEM-like phenomena have been carried out by Gardner [1], Hynes and Gardner [2], and Mensa [4]. There has been significant industrial effort in exploiting JEM for radar target identification, but most of this work has been proprietary.

Typically, JEM target identification processors are spectral analyzers that estimate the periodogram of the target aircraft return in order to extract Doppler information imparted on the scattered electromagnetic field by the rotational motion of the jet engine components. They may employ additional processing (e.g., cepstral processing, time or frequency scaling, etc.) in order to extract information more easily used in the classification algorithms, but spectral analysis is the fundamental basis of their operation. The estimated periodograms are then classified into particular target classes using standard pattern recognition techniques [9–11].

Most investigations of JEM have been experimental in nature and have not placed great emphasis on the modeling of the phenomenon. This is understandable, since the goal of most studies has been to develop radar target identification capabilities for a particular radar system. As a result, the typical approach is an empirical classification of JEM spectra using windowed

periodogram estimates. Generally, this approach has been quite successful, particularly if there were no significant constraints on the allowed radar observation time.

However, in many situations where JEM-based target identification would be useful, it is not feasible to allow long observation times. For example, in air defense surveillance radar, JEM target identification capabilities could be used to determine the type of approaching aircraft. However, air defense radar systems typically have stringent search schedule requirements on their designated search volume. The radar observation time required to identify incoming jet aircraft by analyzing its JEM signature can significantly detract from its surveillance time and energy budget. The development of parametric models accurately describing the JEM process could allow for reliable target identification with a shorter observation time than is possible using periodogram estimates. Such a model-based approach, for example, allows for frequency resolution of autoregressive (AR) processes that is greater than that provided by periodogram methods [12]. Since JEM target identification is based on estimates of the JEM spectrum, and since achieving sufficient Doppler spectral resolution is a limiting factor in the success of JEM target identification, parametric modeling should make it possible to reduce the required observation time.

Here we consider the problem of modeling JEM returns and examine the characteristics of measured JEM signals. In Section II, we consider the problem of modeling JEM returns. We do this first by considering the scattering properties of the *JEM-generating structure* (JGS) when it is stationary and modeling its scattering response to general transmitted waveforms $x(t)$, both for sinusoidal and general transient $x(t)$. These results are useful for understanding the continuity of scattering center motion for sinusoidal radar illumination, which forms the physical basis of our JEM model. It also provides insight into the JGS scattering response for wideband waveforms or narrowband waveforms at different carrier frequencies. Next we consider the problem of characterizing the scattering when the JGS is put into rotational harmonic motion. We note the scattering mechanism by which a periodic modulation is imparted on the scattered waveform and propose a general model for characterizing scattered JEM waveforms.

We then examine the problem of modeling JEM in the more specialized case of making JEM measurements with a radar operating at a single transmitting frequency, corresponding to a pulse Doppler radar system with (relatively) narrowband pulse waveforms. This model is appropriate for the radar measurements we present. In this case, we note that the overall JEM can be decomposed into an amplitude modulation (AM) component and an angle (phase or frequency) modulation component, and that

these two components can be considered separately without loss of generality.

In Section III, we present measurements of JEM made using a modified Hughes pulse-Doppler radar system. After discussing the characteristics of the radar system relevant to JEM measurement, we examine the characteristics of the measured JEM signatures, compare them with the JEM model presented in Section II, and present some of the difficulties involved in measuring the phase-modulation model parameters as a result of sample aliasing and phase ambiguities for phase excursions outside of the interval $[0, 2\pi)$. Then we consider the characteristics of the measured JEM signatures useful for radar target identification.

Finally, in Section IV, we summarize the results of our study to this point and outline further problems that need to be considered in JEM modeling.

II. MODELING OF JEM SCATTERING STRUCTURE

A. General Considerations in Modeling JEM

We first examine the scattering characteristics of the JGS when it is *not* in motion. Assume that the JGS is at a sufficient distance R from the radar illuminator that the magnitude of the illuminating field is constant over the scattering body (i.e., $\sqrt[3]{V_{JGS}} \ll R$, where V_{JGS} is the volume enclosing the JGS) and that the transverse extent of the body is small compared with the first Fresnel zone of the antenna aperture (i.e., ΔX and $\Delta Y \ll \sqrt{R\lambda}$, where ΔX and ΔY are the transverse dimensions of the JGS, and λ is the wavelength of illumination). This being the case, the stationary JGS can be characterized by a scattering distribution $\gamma(r)$ [5, 6]. The distribution $\gamma(r)$ has the interpretation of being the intensity per unit volume of the backscattered electric field at spatial position r. It is thus proportional to the scattering density per unit volume at the point r. Since $\gamma(r)$ is a function defined in three-dimensional (3-D) space, we can decompose it into its Fourier components $A(\mathbf{K})$, where $\mathbf{K} = 2\mathbf{k}$ is the wave vector difference between the scattered wave and the incident wave, and $\mathbf{k} = (2\pi/\lambda)\hat{r}_{rs}$, where $\hat{r}_{rs}$ is the unit vector pointing from the radar aperture to the scatterer. The received electric field $E(\mathbf{K})$ can be written as

$$E(\mathbf{K}) \propto \int_{V_{JGS}} \gamma(r) e^{-i <r|\mathbf{K}>} dr.$$

From this expression, we note that $E(\mathbf{K})$ is continuous in $\mathbf{K}$ for any $\gamma(r)$ confined to a finite region of $\mathbf{R}^3$ as a consequence of fundamental properties of Fourier wave synthesis using a wavevector region of finite support. Our goal in examining this expression is to understand the frequency response behavior of a complex stationary scattering structure. This allows characterization of the JGS scattering

characteristics for a wide variety of illuminating radar waveforms.

This problem can be moved strictly into the time domain. Under the radar-target scenario outlined above, the interference pattern received at the radar antenna is strictly a function of the distance of the elemental scatterers of the extended target from the antenna. If an impulsive plane wave is transmitted by the radar, the received signal $h(t)$ received is characterized by the round-trip time delay and magnitude of the constituent elemental scatterers as observed by the radar for fixed transmit and receive antenna polarizations. So $h(t)$ is effectively a *target impulse response* [13]. Hence, if the transmitted waveform is $e(t)$ and the received waveform is $v(t)$, then

$$v(t) = \int_{-\infty}^{\infty} e(\tau)h(t - \tau)\,d\tau.$$

When the JGS is in motion, it can no longer be described by a linear time-invariant system. The scattering process is still linear, but now it is time varying.

The physics of our particular problem allows for some simplification over that of a general time-varying linear system. For a given illumination frequency and fixed position of the JGS, the returned electric field is equivalent to that of a point target of the proper reflectivity and at the proper range. If the individual elemental scatterers of the JGS are physically moved in a continuous manner, both the phase and the amplitude of the received field scattered from each element changes in a continuous manner. Hence, continuous motion of the JGS results in a continuous change in the received electric field, since the sum of a finite number of continuous functions is itself a continuous function. Here, by "continuous motion" we mean that the motion is constrained such that the component of the scattered field contributed by each individual scatterer changes both continuously in amplitude and phase.

The significance of the continuity of the scattered electric field with continuous motion of the JGS is that the effective scattering center (the point target which characterizes the return from the JGS) changes continuously with the motion of the JGS. This means that since in practice the motion of the JGS is periodic, the motion and amplitude of the effective scattering center of the JGS is also periodic. So, we can characterize JEM as a general periodic modulation, assuming we have compensated for the Doppler shift resulting from radial aircraft motion.

Consider the JEM imparted on a sinusoidal radar waveform of frequency f_0. In general, the received waveform $x(t)$ can have both AM and angle modulation due to JEM. Hence we can write $x(t)$ as

$$x(t) = a(t)e^{i2\pi f_0 t + i\phi(t)}. \tag{1}$$

Here $a(t)$ is the amplitude modulation (*AM*) *function* and $\phi(t)$ is the *phase-modulation function* for the observed signal. In general, $a(t)$ and $\phi(t)$ are a function of the transmitter frequency f_0. We can rewrite $x(t)$ as

$$x(t) = a(t)e^{i\phi(t)}e^{i2\pi f_0 t}$$

$$= z(t)e^{i2\pi f_0 t} \tag{2}$$

where $z(t) = a(t)\exp[i\phi(t)]$ is the *complex envelope* of $x(t)$. Since, as we can see from (2), the spectrum of $x(t)$ is a frequency-shifted version of the spectrum of $z(t)$, it suffices to consider the spectrum of the complex envelope $z(t)$ in order to determine the characteristics of the JEM spectrum.

The complex envelope $z(t)$ is made up of the product of the functions $a(t)$ and $w(t) = \exp[i\phi(t)]$. That is,

$$z(t) = a(t)e^{i\phi(t)}$$

$$= a(t)w(t). \tag{3}$$

We can determine the spectrum $Z(f)$ of $z(t)$ from the spectrum $A(f)$ of $a(t)$ and the spectrum $W(f)$ of $w(t)$, since by the convolution theorem of Fourier transforms,

$$\int_{-\infty}^{\infty} a(t)w(t)e^{-i2\pi f t}\,dt = A(f) * W(f)$$

and thus

$$Z(f) = A(f) * W(f)$$

$$= \int_{-\infty}^{\infty} A(\hat{f})W(f - \hat{f})\,d\hat{f}. \tag{4}$$

Since JEM is a periodic time-varying process, the complex envelope $z(t) = a(t)\exp[i\phi(t)]$ is a time-varying function. If this periodic JEM process has period T_p, then the functions $a(t)$ and $\phi(t)$ are also periodic with period T_p.

Since $a(t)$ is periodic in t with period T_p, we can express $a(t)$ with a complex-exponential Fourier series of the form

$$a(t) = \sum_{n=-\infty}^{\infty} a_n e^{i2\pi f_p n t}, \tag{5}$$

where $f_p = 1/T_p$. The Fourier coefficients $\{a_n\}$ are given by

$$a_n = \frac{1}{T_p} \int_0^{T_p} a(t)e^{-i2\pi f_p n t}\,dt. \tag{6}$$

Taking the Fourier transform of $a(t)$, assuming the order of integration and summation can be exchanged,

we have

$$A(f) = \int_{-\infty}^{\infty} a(t)e^{-i2\pi ft} dt$$

$$= \int_{-\infty}^{\infty} \left[\sum_{k=-\infty}^{\infty} a_n e^{i2\pi f_p kt} \right] e^{-i2\pi ft} dt$$

$$= \sum_{k=-\infty}^{\infty} a_n \int_{-\infty}^{\infty} e^{i2\pi [f_p k - f]t} dt$$

$$= \sum_{k=-\infty}^{\infty} a_n \delta(f - f_p k). \qquad (7)$$

We note that since $a(t)$ is a real function, the coefficients $\{a_n\}$ are conjugate-symmetric in n. We note as well that the resulting spectrum $A(f)$ is a line spectrum with spectral lines occurring at frequencies that are integer multiples of $f_p = 1/T_p$.

We now turn our attention to the angle modulation component $w(t)$ and its spectrum $W(f)$. Since $\phi(t)$ is periodic with period T_p and hence its fundamental frequency $f_p = 1/T_p$, we can express it as a Fourier series in real-polar form:

$$\phi(t) = \sum_{n=0}^{\infty} \beta_n \sin(2\pi f_p nt + \psi_n). \qquad (8)$$

Here β_n is the Fourier magnitude coefficient and ψ_n is the phase angle of the nth harmonic. We approximate $\phi(t)$ by the function $\hat{\phi}_M(t)$, the function made up of the Mth order partial sum of (8):

$$\hat{\phi}_M(t) = \sum_{n=1}^{M} \beta_n \sin(2\pi f_p nt + \psi_n).$$

It can be shown [14, ch. 14] that $e^{i\hat{\phi}_M(t)}$ can be written as the Fourier series expansion

$$e^{i\hat{\phi}_M(t)} = \sum_{k_1=-\infty}^{\infty} \cdots \sum_{k_M=-\infty}^{\infty} \left[\prod_{j=1}^{M} J_{k_j}(\beta_j) \right]$$

$$\times \exp\left[i\sum_{m=1}^{M} k_m \psi_m \right] \exp\left[i\sum_{m=1}^{M} 2\pi f_p k_m t \right].$$

Hence the waveform $w(t)$ is approximately

$$w(t) \approx \sum_{k_1=-\infty}^{\infty} \cdots \sum_{k_M=-\infty}^{\infty} \left[\prod_{j=1}^{M} J_{k_j}(\beta_j) \right]$$

$$\times \exp\left[i\sum_{m=1}^{M} k_m \psi_m \right] \exp\left[i\sum_{m=1}^{M} 2\pi f_p k_m t \right]. \qquad (9)$$

Here $J_k(\cdot)$ is a kth order Bessel function of the first kind.

Since by selecting M sufficiently large, the mean-square error of this approximation can be made arbitrarily small, we assume it is an equality. Then by

calculation of the Fourier transform of the right side of (9), we have that the spectrum $W(f)$ of $w(t)$ is

$$W(f) = \sum_{l=-\infty}^{\infty} \gamma_l \delta(f - lf_p) \qquad (10)$$

where

$$\gamma_l = \sum_{(k_1,\dots,k_M)\in S_l} \left\{ \left[\prod_{j=1}^{M} J_{k_j}(\beta_j) \right] \exp\left[i\sum_{m=1}^{M} k_m \psi_m \right] \right\} \qquad (11)$$

and S_l is the set if all M-tuples of integers whose sum is l.

Our parametric model for the JEM spectrum, is presented in (1) through (11). The model is an idealization in the sense that the JEM return is assumed to be perfectly periodic. In practice, we expect that due to variations in target aspect as a function of time, the modulation may not be perfectly periodic over many periods. However, as the measured data indicates, the return from the JGS appears periodic over several rotation periods.

Note that both the AM and phase-modulation factors in $z(t)$ produce line spectra with frequency lines which are integer multiples of the frequency f_p corresponding to the JEM phenomenon period of T_p (cf., (7) and (10)). Note in particular that the offset frequencies of the sidebands from the carrier in the angle modulation are determined by the JGS rotation frequency and are independent of the radar transmission frequency f_0. Changing the frequency of transmission f_0 does, however, change the magnitude of the phase-modulation indices $\beta_1 \dots, \beta_M$ (from the physics of the Doppler effect, the β_n are proportional to f_0) and this, in turn, changes the Fourier coefficients $\{\gamma_l\}$ as can be seen in (11). Since $Z(f)$ is the convolution of two line spectra with frequency components at integer multiples of f_p, $Z(f)$ is also a line spectrum with frequency components at integer multiples of f_p.

In order to gain intuitive insight into the nature of angle modulation in JEM, we examine an example with a simple sinusoidal $\phi(t)$

$$\phi(t) = \beta \sin 2\pi f_p t. \qquad (12)$$

This corresponds to the scattering center of the JEM-producing mechanism varying its range in a sinusoidal manner, that with respect to some reference range R_0, the range from the target to the radar is given by $R_0 + D/2 \sin 2\pi f_p t$. Here D is the length of the path over which the sinusoidally varying scattering center moves in range, and corresponds to the total range deviation or "range glint" due to the harmonic motion of the scattering center of the JEM-producing scatterers. The modulation index β at a transmitter

frequency of f_0 is

$$\beta = \frac{Df_0}{2c} = \frac{D}{2\lambda}. \tag{13}$$

Hence,

$$\phi(t) = \frac{Df_0}{2c}\sin 2\pi f_p t.$$

Here c is the speed of light and λ is the wavelength of the transmitted waveform. It would be naive to assume that the phase modulation present in JEM can be realistically modeled as a sinusoidal motion of the JGS scattering center in range. In general, we would expect $\hat{\phi}_M(t)$ to have many terms in order to be a reasonable approximation of the $\phi(t)$ corresponding to a real JEM signal. However, this single sinusoid example does provide insight into the angle modulation characteristics of JEM.

In this case, $W(f)$ as given in (10) and (11) simplifies to

$$W(f) = \sum_{k=-\infty}^{\infty} J_k(\beta)\delta(f - f_p). \tag{14}$$

In order to determine the characteristics of this line spectrum, we consider some properties of Bessel functions of the first kind [15, ch. 4].

The first point we note is that the Bessel functions $\{J_k(\cdot)\}$ have the following symmetry/antisymmetry property in k:

$$J_k(\cdot) = \begin{cases} J_{-k}(\cdot), & \text{for } k \text{ odd;} \\ -J_{-k}(\cdot), & \text{for } k \text{ even.} \end{cases} \tag{15}$$

Next we note that for $\beta \ll 1$,

$$J_0(\beta) \approx 1,$$

$$J_1(\beta) \approx \frac{\beta}{2}, \tag{16}$$

$$J_k(\beta) \approx 0, \quad \text{for } k > 1.$$

Finally, we note that asymptotically,

$$J_k(\beta) \sim \left(\frac{2}{\pi\beta}\right)^{1/2}\cos\left(\beta - \frac{k\pi}{2} - \frac{\pi}{4}\right), \qquad \beta \to \infty \tag{17}$$

For a small modulation coefficient $\beta \ll 0$, we have from (14), (15), and (16) that

$$W(f) \approx \delta(t) + \frac{\beta}{2}\delta(f - f_p) - \frac{\beta}{2}\delta(f + f_p). \tag{18}$$

A plot of this line spectrum appears in Fig. 1(a). Note that most of the energy is in the $f = 0$ spectral line with a small portion of the energy distributed asymmetrically in the spectrum between the spectral lines at frequencies $f = f_p$ and $f = -f_p$.

For a modulation index $\beta \gg 1$, we can see from (17) that energy is distributed somewhat equally among a large number of spectral lines. Using Carson's
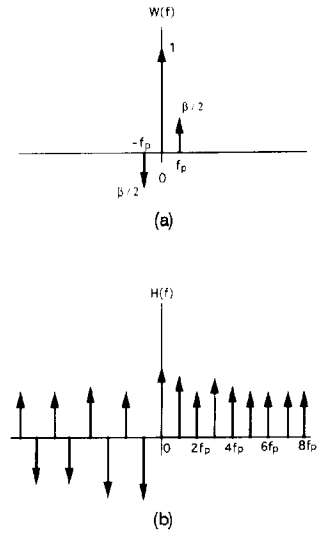

Fig. 1. (a) Spectrum $H(f)$ for $\beta \ll 1$. (b) Spectrum $H(f)$ for $\beta \gg 1$.

approximation for wideband FM, it can be shown that the energy is distributed approximately over the frequency band $[-\beta f_p, \beta f_p]$ [16]. A plot of such a spectrum $W(f)$ is shown in Fig. 1(b).

The spectrum $Z(f)$ of the complex JEM envelope $z(t)$ is the convolution of $W(f)$ with the AM spectrum $A(f)$. Thus for $\beta \ll 1$, we have that

$$Z(f) \approx A(f). \tag{19}$$

As β becomes larger but is still substantially less than one, we have that the JEM spectrum becomes slightly asymmetric. This can be seen by convolving a typical $A(f)$ with the resulting $W(f)$ in these circumstances. This is shown in Fig. 2.

Some investigators of JEM have suggested that JEM is primarily an AM phenomenon. Others have, however, noted the presence of slight asymmetries in some JEM spectra which would not be present in a purely amplitude modulated signal. As was noted in the example above, one possible and likely source of this asymmetry is the presence of angle modulation due to the periodic motion of the scattering center of the JEM generating structure. As noted in the above example, even low modulation index angle modulation can generate significant asymmetries in JEM spectra. In general, as the angle modulation indices β_i increase toward 1 and then become larger, the angle modulation spectrum contains asymmetries that produce an overall asymmetric JEM spectrum $Z(f)$. Unfortunately, the degree of symmetry is not a reliable indicator of the modulation indices. The reason for this is that for $\phi(t)$ with even moderate harmonic content, the intermodulation products generated by the nonlinear phase-modulation process result in a large number of intermodulation-pair
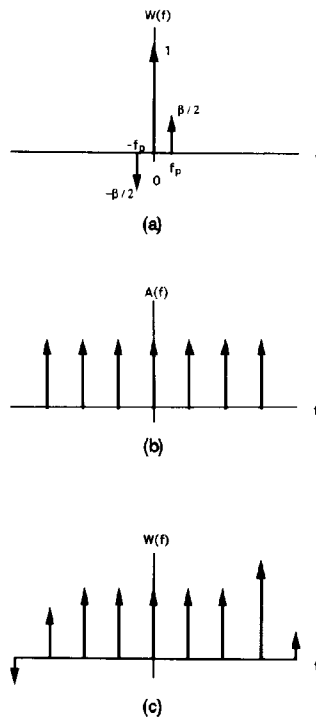
(a)

(b)

(c)

Fig. 2. (a) Spectrum $H(f)$ for $\beta \ll 1$. (b) Spectrum $A(f)$. (c) Spectrum $Z(f) = A(f) * W(f)$.

Fig. 3. Quadrature detector model for pulse-Doppler radar receiver.

contributors to each spectral line in $W(f)$, as can be seen from (10) and (11).

In general, we do not expect $\phi(t)$ to be sinusoidal as in our example, but it is periodic in T_p and can thus be represented by a Fourier expansion of $\phi(t)$. This very simple example, however, does give insight into how angle modulation can generate asymmetries in the JEM spectrum $W(f)$. It also gives plausibility to the notion that angle modulation plays an important role in JEM, as it explains the asymmetries observed in JEM spectra that cannot be attributed to AM alone.

Recall from (18) that the overall JEM spectrum $Z(f) = A(f) * W(f)$, where $A(f)$ and $W(f)$ are the AM and angle modulation spectra, respectively. Recall as well that, from (7), (8), (10), and (11) that $A(f)$ can be completely characterized by the set of exponential Fourier coefficients $\{a_n\}$ of $a(t)$ and $W(f)$ can be completely characterized the set of polar Fourier coefficients $\{(\beta_n, \psi_n)\}$ of the funciton $\phi(t)$. This means that the JEM signal under considerations can be completely characterized by the Fourier analysis of the signals $a(t)$ and $\phi(t)$. So if we can estimate the functions $a(t)$ and $\phi(t)$ from our radar measurements, we can characterize the observed JEM signal by the Fourier coefficients $\{a_i\}$ and $\{(\beta_n, \psi_n)\}$. From these sets of Fourier coefficients, a useful set of features for target identification can, in principle, be derived, since $\{a_i\}$ and $\{(\beta_n, \psi_n)\}$ completely characterize the jet
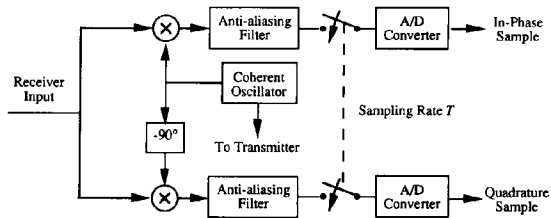
engine induced AM and angle modulation, respectively. Unfortunately, the parameters $\{(\beta_n, \psi_n)\}$ cannot be easily determined from the measured data as is seen when we consider measured data. Thus, although our parametric model provides a useful *forward model* for describing the generation of JEM spectra, the inverse problem associated with parameter estimation in this model is difficult. The primary difficulty with the inverse problem associated with this model is the 2π ambiguity of the phase function when determined from the measured radar data. This, coupled with the fact that aliasing can be present with the PRF-induced (pulse repetition frequency) sampling rate, make the removal of this phase ambiguity difficult. We discuss these problems in Section III. Fortunately, these problems do not destroy all useful data for target identification in the measured data. Hence, target identification based on JEM signatures is possible even if inversion of the model to determine the complete set of descriptive parameters $\{a_n\}$ and $\{(\beta_n, \psi_n)\}$ is not possible.

III. JEM MEASUREMENT WITH A PULSE-DOPPLER RADAR

In our analysis, we are interested in characterizing the AM $a(t)$ and the phase modulation $\phi(t)$ from measurements made using a pulse-Doppler radar with a quadrature detector. The baseband output measurements consist of complex (in-phase and quadrature) samples of the received signal at a sampling rate equivalent to the PRF of the radar system. A block diagram of the quadrature detector model we are considering is shown in Fig. 3.

The pulse-Doppler radar used to make the JEM measurements was a Hughes experimental radar, modified to enable the collection and recording of radar data at a high PRF using long coherent pulse trains. The system is a pulse-Doppler radar system having a rotating phased-array antenna. The phased-array antenna beam is phase-steered in elevation and frequency-steered in azimuth. When an aircraft is acquired and it is desired to make JEM measurements, the radar goes into JEM measurement mode. Here the phase shifters for elevation steering are frozen and a frequency is selected to fix the

TABLE 1
JEM Measurement Radar System Parameters

Parameter	Value
Frequency Band	X-Band
JEM Mode PRF	25 KHz
Antenna Azimuth Beamwidth (3 dB)	2°
Antenna Elevation Beamwidth (3 dB)	2°
Pulse Type	Non-linear FM
Pulse Bandwidth	1 MHz
No. Pulses in JEM-mode Pulse-Train	1024

antenna beam in azimuth with respect to the antenna. The antenna beam is thus frozen with respect to the phase-array antenna aperture. The rotation of the phased-array antenna, however, continues to sweep the antenna beam in azimuth at a constant radial frequency.

The requirement of high pulse repetition translates into a high sampling rate and a resulting high Nyquist frequency. This minimizes the effects of aliasing. However, as we will see, aliasing is still a problem for the wideband angle modulation associated with JEM returns. Table I gives key parameters of the modified radar system.

In order to directly reconstruct $a(t)$ and $\phi(t)$, we must obtain sampled versions $a[n]$ and $\phi[n]$, respectively, at a sufficiently high sampling rate such that aliasing is not a problem. We now investigate this problem in some detail, focusing on $a(t)$ and $\phi(t)$ separately as allowed by the decomposition of (4).

In order to obtain a sampled version $a[n]$ of the envelope signal $a(t)$, we need only take the modulus of the complex sequence formed by the in-phase and quadrature (I and Q) pair samples. That is, if $I[n]$ and $Q[n]$ are the I and Q samples corresponding to the baseband signal $z(t)$, then the complex sample sequence $z[n]$ corresponding to $z(t)$ is given by

$$z[n] = I[n] + iQ[n]$$

$$= a[n]\exp\{i\phi[n]\} \qquad (20)$$

and hence

$$a[n] = \sqrt{|I^2[n] + Q^2[n]|}. \qquad (21)$$

Measurements made on typical jet aircraft with the pulse-Doppler measurement radar indicate that the PRF used corresponds to a sampling rate which is sufficient to represent the AM $a(t)$ with negligible degradation due to aliasing. So $a[n]$ as computed in (21) serves as a sample sequence representative of the envelope $a(t)$. Unfortunately, this is not true in the case of the phase modulation $\phi(t)$.

Examining (20) one might expect that $\phi(t)$ could be represented by the sample sequence $\phi[n] =$

arctan$[Q[n]/I[n]]$. As we will see, this is not generally the case.

As previously noted, the baseband signal $z(t)$ can be written in the form

$$z(t) = a(t)\exp\{i\phi(t)\}.$$

In order to obtain $\phi(t)$, one must take the complex logarithm of the function $w(t) = \exp\{i\phi(t)\}$. Thus

$$i\phi(t) = \log[\exp\{i\phi(t)\}].$$

The problem we encounter when attempting to evaluate this logarithm is that the complex logarithm is not a single-valued function.

For any non-zero number $z = r\exp\{i\theta\}$, the function $\log z$ has infinitely many values. This can be seen by noting the fact that incrementing θ by any interger multiple of 2π does not change the value of z, while it does change the value of $\log z$. Thus

$$\log z = \log r + i(\theta + 2\pi k)$$

for any integer k, and $\log z$ is a multivalued function. In order to determine $\phi(t)$ or its corresponding sample sequence $\phi[n]$ from $(I[n], Q[n])$, we must resolve this multiple of 2π ambiguity.

Now suppose that, for the purpose of illustration, our function $\phi(t)$ is

$$\phi(t) = 3\pi \sin t.$$

Then a plot of $\phi(t)$ would appear as shown in Fig. 4(a). This is a continuous function of t. However, if we take $\phi(t)$ to be the principle value of the complex logarithm of $\log\{i\phi(t)\}$, we get the function shown in Fig. 4(b). This is not a continuous function of t. Let us define this function, the *principle value* (PV) of $\phi(t)$, as $\Phi(t)$:

$$\Phi(t) = \text{PV}\{\phi(t)\} = \phi(t)\bmod 2\pi.$$

From $z(t)$, we can find $\Phi(t)$ given $z(t)$. But we wish to find $\phi(t)$. We simply calculate $\Phi(t)$ as the PV of the argument of $z(t)$ and add or subtract the appropriate multiples of 2π in order to obtain a continuous function. This function is $\phi(t)$. In order to determine the proper multiple of 2π to be added to $\Phi(t)$ in order to obtain $\phi(t)$ we must be able to determine the value of $\Phi(t)$ for all t in some interval $\mathcal{T}$ defined as

$$\mathcal{T} = \{\forall t : \phi(t) \in (2\pi - \epsilon, 2\pi + \epsilon)\},$$

for any $\epsilon > 0$. We can then determine the proper multiple of 2π to be added to $\Phi(t)$ at a given time t in order to determine the value of $\phi(t)$.

This process of adding the proper integer multiples of 2π to $\Phi(t)$ in order to obtain $\phi(t)$ is called *phase unwrapping*. We can define the *phase unwrapping function* $\Upsilon(t;\Phi)$ such that

$$\phi(t) = \Phi(t) + 2\pi\Upsilon(t;\Phi),$$

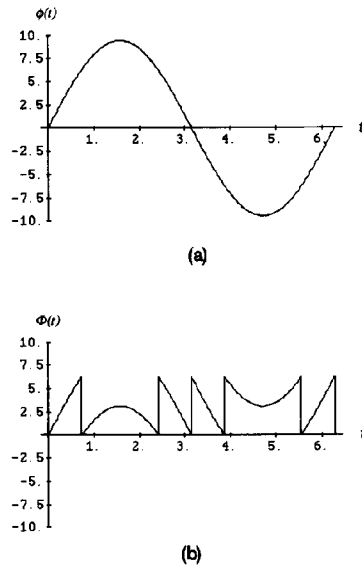where $\Upsilon(t;\Phi)$ takes on the appropriate integer value to make the above relation true.

Fig. 4. (a) $\phi(t) = 3\pi\sin(t)$. (b) $\Phi(t) = 3\pi\sin(t)\bmod 2\pi$.

Our problem in determining the phase function $\phi(t)$ is complicated by the fact that we do not have access to the function $\Phi(t)$, but rather to $\Phi[n]$, a discretely sampled version of it, sampled at a rate corresponding to the PRF of the radar, and given by

$$\Phi[n] = \arctan\left[\frac{Q[n]}{I[n]}\right].$$

Our goal of constructing $\phi(t)$ from $\Phi[n] = \arctan[Q[n]/I[n]]$ is complicated by two facts: 1) The sampling rate may not be sufficient to represent either $\Phi(t)$ and $\phi(t)$ without aliasing. 2) There is a 2π ambiguity in the value of $\phi[n]$ if it is taken to be equal to $\Phi[n]$ as calculated from the measured data.

Note that as a result of the discontinuities in $\Phi(t)$, it generally has greater bandwidth than $\phi(t)$. So even if the PRF-imposed sampling rate is sufficient to represent $\phi(t)$ without aliasing, it may not be sufficient to represent $\Phi(t)$. For the PRF-imposed sampling rates of the experimental measurement radar system, $\Phi(t)$ was found to have too large a bandwidth to apply standard phase unwrapping techniques based on the phase of successive samples. In spite of this, reliable target identification can be performed using this data since most of the information required for target identification is present in the aliased modulo 2π phase samples. Still, phase unwrapping would be useful to better observe and understand the characteristics of JEM from measured data.

We now investigate JEM characteristics using a measurement from the experimental radar system. The measurements were made in the JEM measurement mode with the aircraft at a range of approximately 10 Km. The particular engine on the observed aircraft was known to be a two-stage engine with the first stage
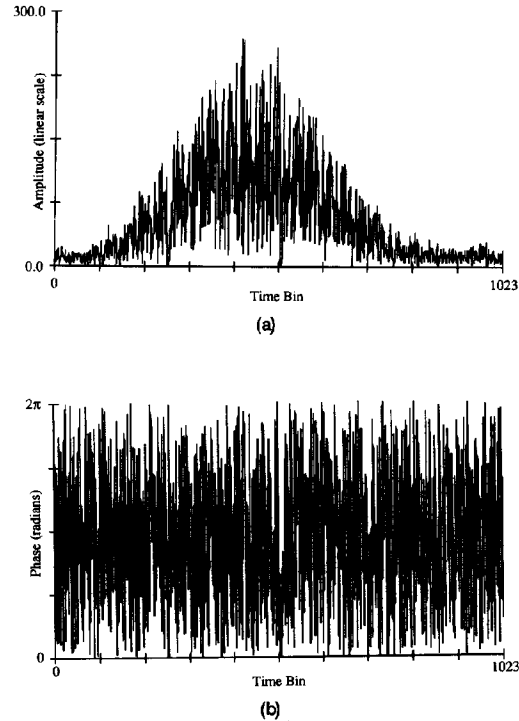

Fig. 5. (a) Amplitude of measured JEM data sequence. (b) Phase of measured JEM sequence.

having a 21-blade fan and the second stage having a 33-blade fan. The aircraft was at sufficient altitude such that clutter returns were not significant problem and so the radar was operated without moving target indicator (MTI) cancellation. The data sequence is made up of 1024 I and Q samples from the quadrature detector. Fig. 5(a) shows a plot of the amplitude sequence $a[n] = \sqrt{I^2[n] + Q^2[n]}$ and Fig. 5(b) shows a plot of the phase sequence $\Phi[n] = \arctan(Q[n]/I[n])$. Note the envelope of the sequence $a[n]$. The windowing of the amplitude data is the result of the antenna pattern being superimposed on the data as the antenna sweeps past the target. In this data, the Doppler offset resulting from the radial motion of the aircraft with respect to the target has been estimated and removed by multiplying the complex data sequence by $\exp(-i2\pi\hat{f}_D n)$, where $\hat{f}_D$ is the estimated radial target Doppler frequency normalized for the radar PRF.

In order to analyze the characteristics of this JEM data, we examine the periodograms and cepstra of the amplitude $a[n]$, the angle modulation sequence $w[n] = \exp\{i\Phi[n]\}$, and the complex envelope sequence $z[n] = a[n]w[n]$. In addition, we find the autocorrelation sequence $R_z[m]$ a useful tool for observing the periodicities present in the complex envelope sequence $z[n]$.

In order to observe the correlation properties of the complex envelope sequence $z[n]$, we use the

unbiased autocorrelation sequence estimate [12]

$$R_z[m] = \frac{1}{N - |m|} \sum_{n=0}^{N-m-1} z[n]z^*[n+m]$$

and then calculate the normalized autocorrelation sequence magnitude given by

$$\hat{r}_z[m] = \left| \frac{R_z[m]}{R_z[0]} \right|.$$

Let the discrete Fourier transform of an N-point sequence be denoted using the operator $\mathcal{F}_N\{\cdot\}$ such that

$$X[k] = \mathcal{F}_N\{x[n]\} = \sum_{n=0}^{N-1} x[n]\exp\{-i2\pi kn/N\},$$

$$k = 0,\ldots,N-1.$$

The corresponding inverse transform can be written as

$$x[n] = \mathcal{F}_N^{-1}\{X[k]\} = \frac{1}{N} \sum_{n=0}^{N-1} X[k]\exp\{i2\pi nk/N\},$$

$$n = 0,\ldots,N-1.$$

The *discrete windowed periodogram* of the sequence $x[n]$ is often used as a crude estimate of its power spectrum; it is defined as

$$\mathcal{P}[k] = \frac{1}{N} \left| \sum_{n=0}^{N-1} x[n]\mu[n]\exp\{-i2\pi kn/N\} \right|^2,$$

$$k = 0,\ldots,N-1.$$

The window function $\mu[n]$ is used to weight the signal $x[n]$ to minimize "leakage" or end effects that result due to the fact that the sequence $x[n]$ being analyzed is not perfectly periodic in N [12]. Note that, as can be seen from Fig. 5, some implicit windowing of the JEM data occurs as a result of the radar antenna pattern and the scanning motion of the antenna.

The *real cepstrum* of the sequence $x[n]$ is used to visualize the presence of periodic components in a signal [17, 18]. It is particularly useful in examining JEM signals. The real cepstrum for the windowed sequence $x[n]$ with window $\mu[n]$ is

$$C_N[n] = \mathcal{F}_N^{-1}\{\log|\mathcal{F}_N\{x[n]\mu[n]\}|\},$$

$$n = 0,\ldots,N-1.$$

We now investigate the autocorrelation sequence, spectra, and cepstra of the measured data to determine if the JEM induced by the jet engine meets our expectations in terms of the JEM model described in (4), (6), (7), (10), and (11).

We first examine the autocorrelation sequence $\hat{r}_z[m]$ of the signal $z[n]$ shown in Fig. 5. This autocorrelation sequence is shown in Fig. 6. It is plotted only for nonnegative m, since $R_z[m]$ is
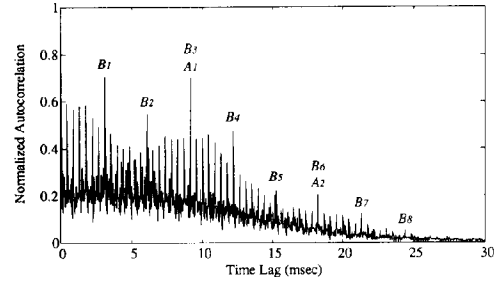

Fig. 6. Normalized autocorrelation sequence $\hat{r}_z[m]$ corresponding to complex envelope sequence $z[n]$.

Hermitian-symmetric, and hence $\hat{r}_z[m]$ is a symmetric sequence in m. Note the strong periodic structure in the signal as indicated by the strong lines in the autocorrelation sequence. The lines indicated with an A(A_1 and A_2) correspond to full-rotation increments of the JGS, whereas the lines indicated with a B($B_1,\ldots,B_8$) correspond to 1/3-rotation increments of the JGS. This form for the correlation sequence is what would be expected from our model, as the data sequence $z[n]$ is assumed to be a finite segment of the sample sequence of a periodic time function $z(t)$. In addition, it is known that for the engine under observation there is a strong symmetry in the JGS at 1/3-rotation, since the number of blades in the two compressor stages has a greatest common divisor (GCD) of 3. The period of rotation corresponding to the A-lines is approximately 9.099 ms whereas the period corresponding to the B-lines is approximately 3.033 ms.

Looking at the next finest set of lines in the correlation sequence, the lines indicated as C-lines, we note that there are 21 C-lines for each A-line, or equivalently, 21 C-lines apparently correspond to the periodic component corresponding to the first-stage fan-blade return. The period of corresponding to the C-lines is 0.433 ms.

The next obvious step would be to look for a finer set of lines in the correlation sequence corresponding to the second-stage compressor fan blades. There should be 33 such lines for each A-line, since there are 33 second-stage compressor blades per revolution of the JGS. The period corresponding to each of these lines is 0.275 ms. These lines are much more difficult to detect visually by observing the autocorrelation function. We can, however, note their presence indirectly through the presence of the strong correlation peak occurring at the period of 1/3-rotation (B-lines). The strong 1/3-rotation symmetry being due to the fact that GCD(21,33) = 3.

We now examine both the spectrum and the cepstrum of the various modulation mechanisms associated with the JEM signature. In Fig. 7, the magnitude of the spectrum and the cepstrum of the complex signal sequence $z[n]$ is displayed. In Fig. 8,
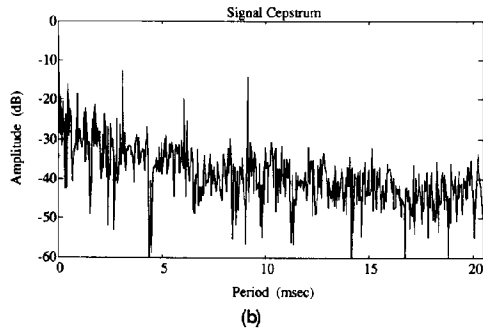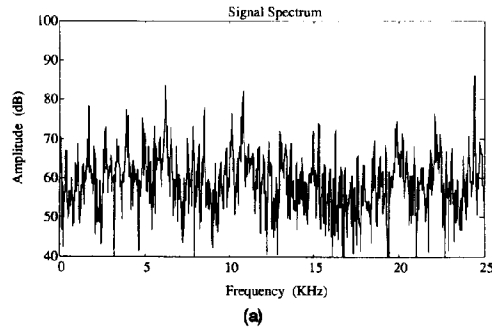
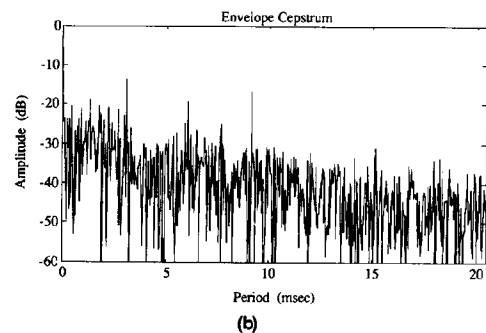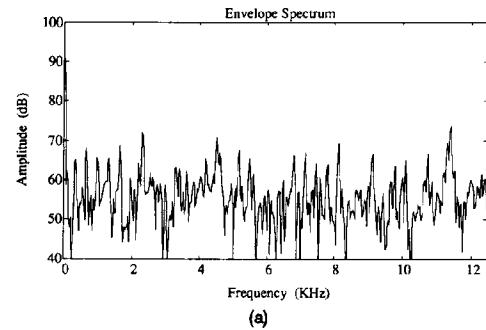Fig. 7. (a) Amplitude of signal spectrum. (b) Signal cepstrum.

Fig. 8. (a) Amplitude of envelope spectrum. (b) Envelope cepstrum.

Fig. 9. (a) Amplitude of phase spectrum. (b) Phase cepstrum.

the magnitude of the spectrum and the cepstrum of the signal envelope sequence $a[n]$ is displayed. In Fig. 9, the magnitude of the spectrum and the cepstrum of the phase sequence $\Phi[n]$ is displayed. In Fig. 10, the magnitude of the spectrum and the cepstrum of the complex phase-modulation sequence $w[n]$ is displayed. In observing the cepstra and spectra for each of these signal sequences related to the JEM signature, we gain insight into the role each plays in conveying information about the observed aircraft engine, providing insight into their relative importance in the design of JEM-based aircraft identification systems.

First we examine the spectrum and cepstrum of the complex signal sequence $z[n]$ as shown in Fig. 7. The spectrum in Fig. 7(a) shows a number of strong spectral lines. Looking at the strongest periodic sequence of these lines, we note that they have a spectral spacing of approximately 2.3 KHz. This is approximately 21 times the fundamental rotation frequency of 110 Hz (corresponding to the A-lines in Fig. 5). The signal cepstrum in Fig. 7(b) shows periodicities corresponding to the A-, B-, and C-lines present in the autocorrelation sequence of Fig. 5.

Next we examine the spectrum and cepstrum of the envelope sequence $a[n]$. These are given in Fig. 8. Examining the amplitude of the envelope spectrum, we once again note the presence of spectral peaks. There are strong spectral peaks at multiples of approximately
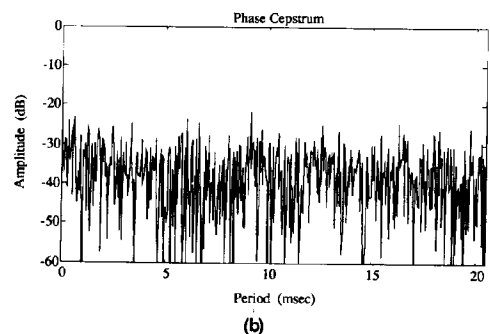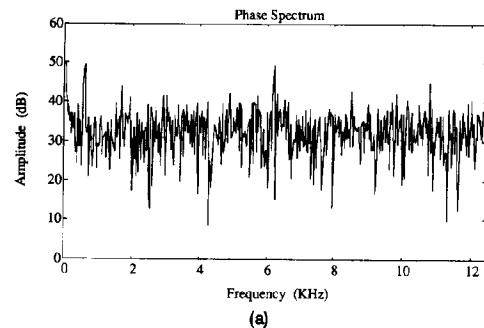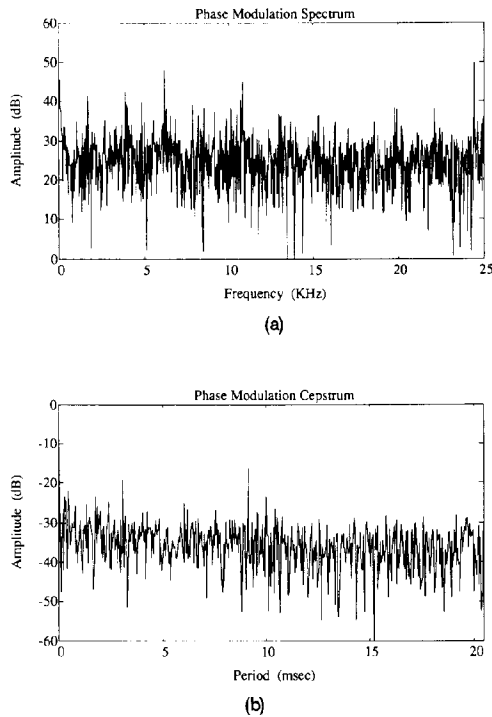
Fig. 10. (a) Amplitude of phase-modulation spectrum.
(b) Phase-modulation cepstrum.

2.3 KHz, the frequency corresponding to 21 times the fundamental frequency of JGS rotation. Note also the presence of harmonic lines at 1/7 this frequency. These lines occur at frequency intervals of approximately 330 Hz, the frequency corresponding to 1/3 of a JGS rotation. The presence of these components is to be expected, considering the strong 1/3 rotation symmetry in the JGS.

Examining the cepstrum of the envelope sequence in Fig. 8(b), we note that it has lines corresponding to the 1/3-rotation symmetry (B-line) and full-rotation symmetry (A-line) periods just as the cepstrum of the signal sequence of Fig. 7(b). Comparing both the spectrum and the cepstrum of the signal sequence (Fig. 7) and the envelope sequence (Fig. 8), it appears that there is more information readily available characterizing the jet engine under observation in the complete signal sequence than in the envelope sequence alone. Thus it appears that there is useful information in the phase sequence $\Phi[n]$ and the phase-modulation sequence $w[n]$. We now examine the spectra and cepstra of these sequences.

The spectrum and the cepstrum of the phase sequence $\Phi[n]$ is shown in Fig. 9. Examination of both the spectrum and cepstrum indicate little of the periodic structure present in the signal sequence $z[n]$ or the envelope sequence $a[n]$. In the phase spectrum of Fig. 9(a), we observe the strongest

spectral peaks occurring at 680 Hz, 6.2 KHz, 8.5 KHz, 9.8 KHz, and 10.8 KHz. Looking back at the signal spectrum, spectral peaks can be observed at all of these frequencies except at 9.8 KHz. In no instance, however, do these frequencies correspond to dominant spectral peaks in the spectrum of the signal sequence $z[n]$. Comparing the frequencies of these peaks in the phase spectrum to those in the envelope spectrum, we note that the only significant corresponding peaks in the envelope spectrum are at 9.8 KHz and 10.8 KHz.

Examining the cepstrum of the phase signal $\Phi[n]$ in Fig. 9, there are very few distinct cepstral lines that stand out. The three cepstral lines corresponding to 1/3-rotation, 2/3-rotation, and one full rotation, which were visible both in the cepstrum of $z[n]$ and the cepstrum of $a[n]$, are clearly visible, but they do not stand out distinctly as in these previous two cases. In general, it appears that it is much more difficult to pick useful information out of the phase's spectrum and cepstrum, but before making this conclusion, we examine the phase-modulation spectrum and cepstrum.

The spectrum and the cepstrum of the phase-modulation sequence $w[n] = \exp\{i\Phi[n]\}$ is shown in Fig. 10. Note that the spectrum and cepstrum of $w[n]$, which is a function of $\Phi[n]$, exhibit many of the same characteristics as the spectrum and cepstrum of the complete signal $z[n]$. Note in particular that the spectrum of $w[n]$ in Fig. 10(a) has dominant spectral peaks at all of the frequencies at which dominant spectral peaks occur in the spectrum of $z[n]$ shown in Fig. 7(a). A visual inspection of the spectrum indicates that most all of the information available in the spectrum of $z[n]$ useful for characterizing the JGS from which this signal arose is also available in the spectrum of the phase-modulation sequence $w[n]$.

Examining the cepstrum of the phase-modulation signal $w[n]$ in Fig. 10(b), we note that the 1/3-rotation period line and the full-rotation period line are clearly visible, just as in the cepstrum of the signal $z[n]$ shown in Fig. 7. Note, however, that the cepstrum of $w[n]$ does not exhibit the 2/3-rotation line as clearly as the cepstrum of the cepstrum of $z[n]$ (Fig. 7(b)). In the cepstrum-based JEM target identification algorithm with which we've experimented, the phase-modulation cepstrum alone was sufficient to accurately identify the observed aircraft type. This was not true of either the envelope cepstrum or the phase cepstrum. This is not to say that the necessary information is not present in the envelope $a[n]$ and phase $\Phi[n]$—indeed the information must be present in $\Phi[n]$ if it is present in $w[n]$—but just that for the particular cepstral-based aircraft identification algorithm with which we experimented, the information was not extractable on a consistent basis from either the cepstrum of $a[n]$ or $\Phi[n]$.

The question arises as to how the JGS harmonic information can be so readily observable in the spectrum and cepstrum of $w[n] = \exp\{i\Phi[n]\}$ but not

in $\Phi[n]$ itself. The answer is found in the fact that $\Phi[n]$ is a phase ambiguous version of the true phase sequence $\phi[n]$:

$$\Phi(t) = \mathrm{PV}\{\phi(t)\} = \phi(t) \bmod 2\pi.$$

Recall that this is the phenomena we saw in the example of a simple sinusoidal phase excursion of the JGS scattering center in Fig. 4 when the total phase excursion is greater than 2π, where a phase change of 2π corresponds to a two-way range change of $\lambda/2$. The net result of this result in the example of Fig. 4 is to take a single frequency sinusoidal waveform $\phi(t)$ and map it into a complex periodic waveform $\Phi(t)$ of significantly wider bandwidth. This same bandwidth expansion process occurs for more complex waveforms $\phi(t)$ as well. Evidence provided by measured waveforms as displayed in Figs. 9 and 10, as well as physical arguments based on the range extent of the JGS and the wavelength of the illuminating radar lead us to believe that phase excursions of many times the 2π phase ambiguity interval are present. Note, however, that this does not change the behavior of the spectrum and cepstrum of $w[n] = \exp\{i\Phi[n]\}$ as in all cases, $\exp\{i\Phi[n]\} = \exp\{i\phi[n]\}$, even though $\Phi[n] \neq \phi[n]$. This is why we still see the correct components in the spectrum and cepstrum of $w[n]$.

IV. DISCUSSION AND CONCLUSIONS

Having proposed a model for JEM signatures, discussed some of its properties, and examined the characteristics of a measured JEM signature, we now present some observations we have made in our modeling and measurement study of the JEM and note their implications to the design and implementation of JEM target identification algorithms in radar systems. We divide this discussion into two major topic areas: summary of modeling and measurements, and implications for JEM target identification.

A. Summary of Modeling and Measurements

We have developed a parametric model for JEM spectra. The model describes the periodic modulation of the signal scattered from the JGS resulting from the periodic motion of the JGS with respect to the airframe being observed. The physical basis for this modeling approach was considered through continuity of motion of the effective scattering center of the JGS with respect to the rotational motion of the JGS for narrowband waveforms. The modulation imparted by the periodic motion of effective scattering center of the JGS with respect to the airframe results in a periodic modulation in the return when we compensate for the airframe radial Doppler component.

We then examined the specific case of JEM signatures for single frequency illumination, noting

that the results are applicable to the analysis of JEM for radars employing narrowband waveforms. We derived expressions for the form of the spectral characteristics of JEM. This is done by noting that the overall spectrum can be decomposed into the envelope spectrum (corresponding to AM imposed on the scattered signal by JGS motion) and the phase-modulation spectrum (corresponding to the phase modulation imposed on the scattered signal by JGS motion). The overall signal spectrum is the convolution of these two spectral components. This allows the spectral characteristics to be completely specified in terms of the spectral characteristics of these two components. We next considered the spectral characteristics of the envelope modulation and phase-modulation components of the JEM signal. We noted that both components consisted of line spectra with a fundamental frequency of $1/T_p$, where T_p is the period of JGS rotation. We derived formulas for the spectral line strengths of the envelope and phase-modulation spectra which corresponded to the spectra amplitude and phase modulation for signals made up of multiple sinusoidal tones. This provided us with a model to study JEM signatures measured with the experimental radar stystem.

Next we examined the JEM signature corresponding to an aircraft track for which the characteristics of the JGS were known. For this track, the autocorrelation sequence of the measured signal, as well as the spectrum and cepstrum of the signal sequence, envelope sequence, phase sequence, and phase modulation sequence all exhibited properties predicted by the JEM model developed here. It was also noted that these features could not be readily observed in the phase sequence, although the information is obviously there because it is present in the phase-modulation sequence, which is a function of the phase sequence. The reason that the information is not easily discernible is the $\bmod 2\pi$ ambiguity in the calculated phase sequence, as discussed in Section III. As we noted, this ambiguity is irrelevant in the mapping from the phase sequence to the phase-modulation sequence. The ambiguity does, however, make it difficult to study the phase sequence in terms of the measured I and Q values measured at the output of the quadrature detector. In fact, this appears to require sophisticated phase unwrapping algorithms which we have not yet successfully developed. Simple phase unwrapping algorithms [18, sect. 10.4] have not been effective. This is most likely due to the fact that it is possible for the scattering center to move more than 2π in phase in a single sampling instant. The development of more effective model-based phase-unwrapping algorithms would allow direct use of the parametric JEM model developed in Section II. In addition, it would allow further study of the phase-modulation characteristics of JEM.

B. Implications for JEM Target Identification

Although the reason for studying JEM signatures is to provide a method for radar target identification, we have said little about the actual pattern recognition techniques that might be used to classify or identify aircraft from their JEM signatures. The details of the various approaches that might be taken are not considered here. References [9, 10, 11, 19] discuss various pattern recognition techniques that may be applied to this problem. A number of approaches, either "low-level" techniques that attempt to identify the target directly by operating directly on the I and Q data or spectral signature of the target, or "high-level" techniques that attempt to extract high-level information about the JGS such as number of engine compressor stages, number of blades per compressor stage fan, GCD between number of blades in each compressor stage fan, engine rotation rate range, etc., and use this information to parse a classification tree [20] or look up the aircraft type in a database, can be applied. A general overview of pattern recognition techniques can be found in [21]. It is also possible that neural networks may provide a possible method of performing the target identification function [22].

When using low-level pattern recognition techniques to identify aircraft, several factors must be kept in mind. First of all, the JGS rotation rate for a given aircraft will vary, since engines are called upon to provide different thrusts under different operating conditions. Thus algorithms based on processing low-level data must compensate for this. Fortunately, the spectral characteristics of the JEM signal as a function of JGS rotation rate are well understood through the modeling presented in Section II. Based on these results, preprocessing to normalize engine rotation rate can be performed by time axis scaling to provide a normalized fundamental frequency of JGS rotation. This greatly simplifies the pattern recognition task for target identification.

The effects of changes in frequency band of operation on low-level JEM descriptions or signatures may provide the single greatest difficulty in applying these techniques to JEM target identification. The ability to map reference signatures of specific aircraft types collected on one radar system to another radar system operating in a completely different frequency band may be important for building a comprehensive database of reference signatures for the particular system on which JEM target identification is to be implemented. Detailed frequency response characteristics of the JGS structures encountered will generally be unavailable (especially for hostile aircraft) and this may present a significant problem for JEM target identification system development.

High-level descriptions or signatures are more robust to changes in operating frequency than low-level descriptions. This is because we are generally dealing with physical characteristics of the JGS that are not a function of observation frequency. However, some of these high-level descriptions may be more easily determined at some observation frequencies than at others. Even if only some of the high-level descriptors can be reliably determined, it may still be possible to reliably identify a target based on a partial list of descriptors. This fact, coupled with the ease of mapping high-level descriptions from one frequency band to another make the high-level approach seem very attractive. The question then becomes one of what types of features should be included in the high-level description. We have already mentioned several and have actually gone through the process of manually extracting them when we examined the plots in Figs. 5–10. In particular, it appears that the signal autocorrelation function and either the signal cepstrum or phase-modulation cepstrum are most useful for this purpose. Still, robust algorithms for extracting these descriptors must be developed if a high-level JEM based target identification system is to be reliable.

The primary reason for considering parametric modeling of JEM signals relates to the fact that with accurate parametric models of a signal being analyzed, it is possible to obtain better estimates characterizing the signal for a given signal sequence length than when using a nonparametric technique. As an example of this, consider the example of AR spectral estimation [12]. It is well known that, for an observed signal sequence of fixed length, if the observed signal can be accurately modeled as an AR process, it is possible to get much higher resolution power spectral density (PSD) estimates of the signal using an AR spectral estimation technique than when using a nonparametric technique of power spectral estimation such as a periodogram or Welch estimate of the PSD. This fact is directly applicable to PSD-based JEM target identification algorithms and more generally applicable to all methods of target identification.

Our investigation of JEM target identification algorithms using periodogram spectra and cepstra have indicated that spectral resolution and the abiltity to resolve closely spaced spectral lines is essential for reliable target identification. For the experimental periodogram and cepstrum-based identification algorithms with which we have worked, observation times of 25 ms or more with the experimental radar system allowed for reliable identification between five different aircraft types. For observation times less than this, identification performance deteriorated rapidly. We believe that these failures can be attributed to a loss in spectral resolution in the periodogram of the JEM signal resulting from decreased observation time, although a detailed analysis of these effects has not been carried out. Note that in order to obtain a

25 ms time-on-target for the experimental radar system with a nominal azimuth antenna bandwidth of 2° requires an antenna revolution period of approximately 4.5 s. In fact, one of the modifications made to the experimental radar system was an antenna drive gear ratio reduction to slow the antenna rotation rate to 1/3 its original rate so that sufficiently long observation times could be achieved. This is too slow a scan rate for most air defense applications. As a result of the problems arising from the long observation times required when using nonparametric spectral estimates, it seems reasonable to attempt to reduce the observation time using parametric models.

In examining parametric models for use in modeling JEM for use in parametric estimation, perhaps the most obvious model to use would be the model developed in Section II, described by (4), (6), (7), (10), and (11). However, least-squares estimation of the phase parameters $\{\beta_n, \psi_n\}$ from either $w[n]$ or the ambiguous phase sequence $\Phi[n]$ is a difficult nonlinear least-squares problem, and finding the solution $\{\hat{\beta}_1...,\hat{\beta}_M,\hat{\psi}_1,...,\hat{\psi}_M\}$ achieving the global minimum square error is not practical for even moderate values of M. One solution to this problem would be to develop an effective phase unwrapping algorithm to obtain the unambiguous phase sequence $\phi[n]$ from $\Phi[n]$. Such a phase unwrapping algorithm that can reliably perform this task has not been found. Instead of using the proposed parametric model for estimation purposes, it may be possible to use others which are more computationally manageable.

Since the JEM spectrum is a line spectrum with strong harmonic lines, one possible parametric model that may be useful is the AR random process model [12]. The AR model is well suited to modeling the sharp spectral peaks present in the JEM spectrum. In addition, a number of computationally efficient algorithms exist for calculating the AR model parameters. These parameters could then possibly be used as target identification features in a low-level description using shorter observation times. Such techniques may have the potential to make JEM target identification a practical target identification technique for air defense radar systems.

ACKNOWLEDGMENT

REFERENCES

[1]   Gardner, R. E. (1961)
       Report 5656, Naval Research Laboratory, Washington, DC,
       Aug. 1961.

[2]   Hynes, R., and Gardner, R. E. (1967)
       Doppler spectra of S band and X band signals.
       EASTCON 1967, Supplement to IEEE Transactions on
       Aerospace and Electronic Systems, AES-3, 6 (Nov. 1967),
       356–365.

[3]   Skolnik, M. I. (1970)
       Radar Handbook.
       New York: McGraw-Hill, 1970.

[4]   Fliss, G. G., and Mensa, D. L. (1986)
       Instrumentation for RCS measurements of modulation
       spectra of aircraft blades.
       In Proceedings of the IEEE 1986 National Radar
       Conference, Los Angeles, Mar. 12–13, 1986.

[5]   Gjessing, D. T. (1986)
       Target Adaptive Matched Illumination Radar: Principles
       and Applications.
       London, Peregrinus, Ltd., 1986.

[6]   Blackridge, J. M. (1989)
       Quantitative Coherent Imaging.
       New York: Academic Press, 1989.

[7]   Bell, M. R. (1988)
       Information theory and radar: Mutual information and the
       design and analysis of radar waveforms and systems.
       Ph.D. dissertation, California Institute of Technology,
       Pasadena, 1988.

[8]   Bell, M. R. (1993)
       Information theory and radar waveform design.
       To appear in IEEE Transactions on Information Theory.

[9]   Duda, R. O., and Hart, P. E. (1973)
       Pattern Classification and Scene Analysis.
       New York: Wiley, 1973.

[10]   Simon, J. C. (1986)
       Patterns and Operators.
       New York: McGraw-Hill, 1986.

[11]   Therrien, C. T. (1989)
       Decision, Estimation, and Classification.
       New York: Wiley, 1989.

[12]   Marple, S. L. (1987)
       Digital Spectral Analysis with Applications.
       Englewood Cliffs, NJ: Prentice-Hall, 1987.

[13]   Ruck, G. T., Barrick, D. E., Stuart, W. D., and Krichbaum,
       C. K. (1970)
       Radar Cross Section Handbook.
       New York: Plenum, 1970.

[14]   Middleton, D. (1960)
       Introduction to Statistical Communication Theory.
       New York: McGraw-Hill, 1960.

[15]   Hildebrand, F. B. (1976)
       Advanced Calculus for Applications (2nd ed.).
       Englewood Cliffs, NJ: Prentice-Hall, 1976.

[16]   Pierce, J. R., and Posner, E. C. (1980)
       Introduction to Communication Science and Systems.
       New York: Plenem, 1980.

[17]   Rabiner, L. R., and Gold, B. (1975)
       Theory and Application of Digital Signal Processing.
       Englewood Cliffs, NJ: Prentice-Hall, 1975.

[18]   Oppenheim, A. V., and Schafer, R. W. (1975)
       Digital Signal Processing.
       Englewood Cliffs, NJ: Prentice-Hall, 1975.

[19]   Fu, K.-S. (1982)
       Syntactic Pattern Recognition and Applications.
       Englewood Cliffs, NJ: Prentice-Hall, 1982.

[20] Breiman, L., Friedman, J. H., Olshen, R. A., and Stone, C. J. (1984)
    Classification and Regression Trees.
    Belmont, CA: Wadsworth International Group, 1984.

[21] Young, T. Y., and Fu, K. S. (Eds.) (1986)
    Handbook of Pattern Recognition and Image Processing.
    New York: Academic Press, 1986.

[22] Lippmann, R. P. (1987)
    An introduction to computing with neural nets.
    IEEE Transactions on Acoustics, Speech, and Signal Processing (Apr. 1987).

Mark R. Bell was born in Long Beach, CA, in 1959. He received the B.S. degree in electrical engineering from California State University Long Beach, in 1981 and the M.S. and Ph.D. degrees in electrical engineering from California Institute of Technology, Pasadena, in 1982 and 1988, respectively.

From 1979–1988, he was employed by Hughes Aircraft Company, Fullerton, CA. From 1981–1988, he was affiliated with the Radar Systems Laboratory at Hughes, where he held the positions of Member of the Technical Staff and Staff Engineer, working in the areas of radar signal processing, electromagnetic scattering, radar target identification, and radar systems analysis. While at Caltech, he held a Hughes Masters Fellowship from 1981–1982 and a Hughes Doctoral Fellowship from 1984–1988. Since August 1989, he has been on the faculty of Purdue University, West Lafayette, IN, where he is an Assistant Professor in the School of Electrical Engineering. His research interests are in the areas of information theory, source coding, synthetic aperture radar, and radar and sonar signal processing.

Dr. Bell is a member of Tau Beta Pi, Eta Kappa Nu, the American Mathematical Society, and the Society of Photo-Optical Instrumentation Engineers.

Robert A. Grubbs received the A.S. degree in ground radar technology from the Community College of the Air Force, the B.S. degree in engineering from California State University Fullerton, and the M.S. degree in electrical engineering from the University of Southern California, Los Angeles, in 1979, 1983, and 1986, respectively.

From 1972–1979 he was an Air Traffic Control Radar Technician with the United States Air Force. From 1979–1980 he was a radio technician with Travel Electronics, Irvine, CA. From 1980–1989, he was employed by Hughes Aircraft Company, Ground Systems Group, Fullerton, CA. From 1980–1983 he worked as a student engineer and was a Hughes Bachelors Scholar. From 1983–1985 he was a member of the Technical Staff and a Hughes Masters Fellow at the University of Southern California. From 1985–1989 he was a Group Head, Target Identification Group in the Tactical Radar Systems Department. Since October 1989, he has been a Staff Engineer with Martin Marietta Advanced Development and Technology Operations, San Diego, CA, where he has been involved in the design, analysis, and testing of prototype radar, sonar, and infrared surveillance systems.